International Journal of Electrical and Electronics Research ISSN 2348-6988 (online)
Vol. 3, Issue 3, pp: (21-34), Month: July - September 2015, Available at: www.researchpublish.com

MULTI-INPUTPORT FULL BRIDGE BIDIRECTIONAL DC-DC CONVERTER FOR RENEWABLE ENERGY BASED DC DRIVE

[1]Dr. P. SELVAM, [2]S.SUBRAMANIAN, [3]G.RAMAKRISHNA PRABU

[1]HOD/EEE, [2]II-YEAR ME., [3]ASSOCIATE PROF./EEE

[1, 2, 3] V.M.K.V. Engineering college, Periyaseeragapadi, Salem

Abstract: **A systematic method for deriving multiport converters (MPCs) from the full bridge (FB) converter (FBC) and bidirectional dc–dc converters (BDCs) is proposed in this paper through sharing the parasitized switching legs by the BDCs and the FBC. By employing the proposed method, families of FB and BDC-based MPCs (FB-BDC-MPCs), including some existing ones, are developed for renewable generation systems with the merits of simple topology, reduced devices, and single-stage power conversion. Voltage regulations between any two ports can be achieved by employing pulse width modulation and phase-angle shift control scheme. Furthermore, zero-voltage switching for all the switches can be realized in the proposed FB-BDC-MPCs. A typical four-port converter developed by the proposed method, named buck/boost four-port converter (BB-FPC), is analyzed in detail as an example in terms of operation principles, design considerations, and control strategy. Experiment results have been carried out on a prototype of BB-FPC, which demonstrate the feasibility and effectiveness of the proposed topology derivation method.**

Keywords: **Bidirectional dc–dc converter (BDC), full-bridge converter (FBC), multiport converter (MPC), renewable power based servo Drive.**

I. INTRODUCTION

RENEWABLE sources are intermittent in nature. To smoothly supply loads, storage elements, functioning as an energy buffer, are needed in a stand-alone renewable power system, where several separate dc–dc converters are conventionally employed. These systems may have the drawbacks of high cost and low efficiency due to multiple stage conversion. MPCs, which are capable of interfacing and controlling several power terminals synergistically and have the merits of low cost, high power density, high efficiency, and compact structure, have attracted an increasing research interest recently. An MPC can interface several renewable power sources, such as multichannel PV panels, hybrid PV, and wind turbines, simultaneously. It can implement MPPT for each renewable source individually and help to reduce the impacts of power mismatch among the renewable sources and maximize the output power of the system. Meanwhile, since energy storage systems are usually required to ensure the system stability and improve dynamics and steady-state performances when utility grid is not available, a bidirectional interfacing is necessary for the MPC.

Generally, the MPCs can be classified into three categories: fully isolated topologies, fully nonisolated topologies, and partly isolated topologies. Fully isolated MPCs are typically derived by combining full-bridge, half-bridge, or series-resonant topologies via magnetic coupling, e.g., utilizing multi winding transformers. Isolation and bidirectional capabilities of all the ports and ZVS can be achieved in these topologies. These MPCs are good candidates for the applications where isolation and bidirectional conversion are required. However, the major problem is that too many active switches are used. This results in complicated driving and control circuitry, which may degrade the reliability and

performance of the integrated converters. Nonisolated MPCs can either be derived by using dc-link, or integration method. These MPCs feature compact design and high power density. However, voltage levels of all ports are not flexible, and ZVS cannot be achieved easily. Partly isolated MPCs are based on hybrid topologies of isolated circuits and nonisolated circuits, which can provide the necessary isolation for the load with flexible voltage levels and maintain advantages of compact design and high power density. In a boost-integrated MPC has been presented by combining a PS-FBC and a boost converter. The power flow control has been realized by using PWM plus phase-angle-shift control scheme.

This principle is further applied to the three-phase FBC. These MPCs have some common features, i.e., the structures of the primary side circuit are similar. However, they have only rarely been examined and investigated in terms of their relationships, topological characteristics, or how to derive these topologies.

Note that there are two switching legs in a PS-FBC.On the other hand, the switching leg is also a basic element of a nonisolated BDC. Therefore, the switching leg is a common element of both the FBC and BDC and can be shared by them. From this point of view, a methodology for synthesizing MPCs is inspired by integrating and sharing the switching legs, instead of magnetic coupling or dc link, to realize nonisolated bidirectional conversion and isolated unidirectional conversion with high integration and fewer components. Based on this idea, a systematic method for deriving MPC topologies from FBCs and BDCs is proposed, and novel MPC topologies are developed. These converters are composed of one isolated unidirectional load port and multiple nonisolated bidirectional ports. Furthermore, only four MOSFETs are used in the proposed MPCs, which is the same as in the conventional FBC. Thus, these MPCs have the advantages of simple topology and easy control. The single-stage power conversion between any two of the ports is realized, and the ZVS of all the switches can also be achieved by adopting pulsewidth and phase-angle-shift modulation strategy. The main focus of this paper is to propose a systematic method for the derivation of MPC topologies from FBC and nonisolated BDCs. The derived MPCs, including those proposed in [18]–[20], provide good candidates for the applications of renewable power system, such as PV-supplied aerospace power systems, hybrid energy storage systems, fuelcell and battery systems, and thermoelectric generation systems with battery backup. This paper is organized as follows. In Section II, the derivation methodology of the MPCs is proposed, and families of MPC topologies are derived. In Section III, the BB-FPC is analyzed in detail, including operation principles and design considerations presented. The modulation scheme, operation mode analysis, and power management strategy are presented in Section IV. Experimental results based on real PV–battery power system are presented in Section V. Finally, Section VI concludes this paper.

II. DERIVATION OF THE FB-BDC-MPC

A. Idea of MPC Topology Deriving from FBC and BDCs

The PS-FBC is shown in Fig. 1(a), and the steady-state waveforms of the PS-FBC are illustrated in Fig. 1(b). It can be seen that the sub circuit on the primary side of the

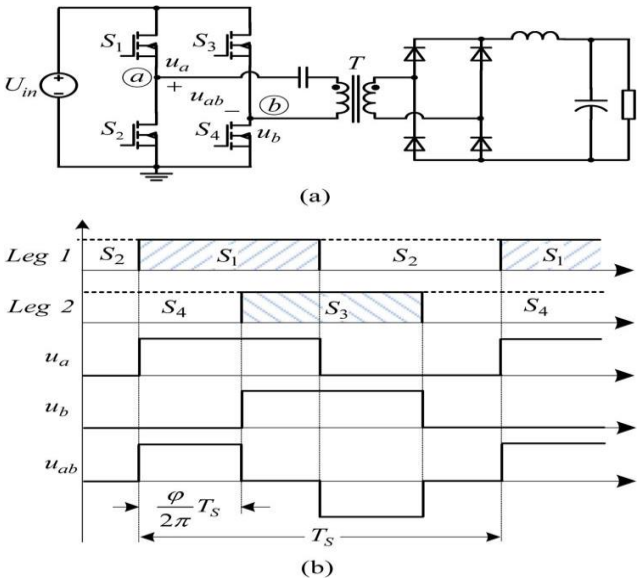

Fig.1. PS-FBC and its operation waveforms (a) FBC (b) Operation waveforms

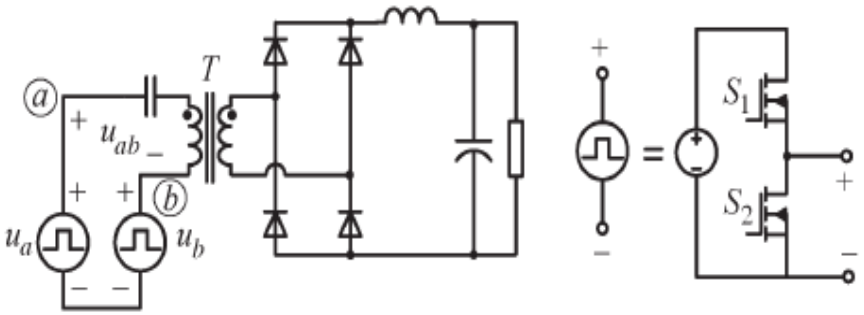

Fig.2. Simplied circuit of the PS-FBC with common negative terminal

PS-FBC is composed of two switching legs and an input source *U*in, and Leg 1 is composed of *S*1 and *S*2 while Leg 2 is composed of *S*3 and *S*4. Each switching leg generates a square-wave voltage, *ua* or *ub*, from *U*in. The two voltages *ua* and *ub* are in phase shift with an angle ϕ to control the voltage on the transformer primary winding, *u*ab. From this viewpoint, the primary subcircuit of the PS-FBC can be simplified into two square-wave voltage sources, as shown in Fig. 2, where the two sources can be connected with a common negative terminal.

On the other hand, we find that the mentioned square-wave voltage sources and the switching leg also exist in a basic nonisolated BDC. As shown in Fig. 3, every BDC has a switching leg, composed of *S*1 and *S*2, in parallel with a dc voltage source, *U*dc. When the two switches, *S*1 and *S*2, operate in the complementary state, a square-wave voltage is generated at the midpoint of the switching leg. It indicates that a square-wave voltage source is parasitized in the BDC. Taking the buck/boost BDC as an example, the parasitized square-wave voltage source is shown in Fig. 4.

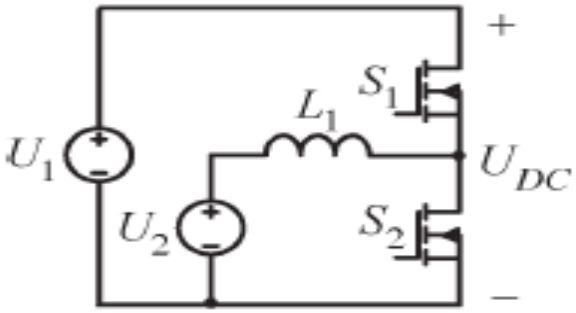

Fig.3. Buck/Boost BDC

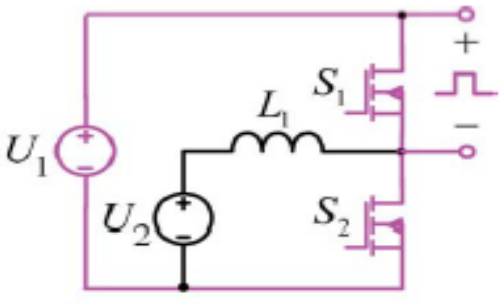

Fig.4. Square-wave voltage source parasitized in the buck/boost BDC

According to the aforementioned observation and analysis, the square-wave voltage source and switching leg are common cells in both the BDCs and FBC. Thus, a method for synthesizing an MPC is inspired by combining the FBC and two BDCs via sharing the common switching cells. With the two square-wave voltage sources parasitized in the BDCs building the primary sub circuit for an FBC, an FB, and BDC-based MPC (FB-BDC-MPC) can be derived. In the derived FB-BDC-MPC, the output voltage of the FBC is controlled by the phase angle shifting between the two legs, and the power exchange between the original ports of the BDC section is regulated by the duty cycle of the leg switches under PWM. Furthermore, to build an FB-BDC-MPC, we just need to connect the two terminals of the transformer primary

winding to the midpoints of two BDCs' switching legs, and the two legs should have at least one common terminal, either the negative or positive one, to form a closed circuit loop for the primary current, as shown in Fig. 2. Following this principle, the generation of an FB-BDC-MPC is illustrated in Fig. 5. It can be seen that, before synthesizing the FB-BDC-MPC topology, the two BDCs contain four voltage sources totally. When an FB-BDC-MPC is built, some of the voltage sources/ports can also be merged and shared by the two BDCs, as shown in Fig. 6, where the two BDCs can be connected in parallel, with a port or a terminal shared.

B. Topologies of the FB-BDC-MPCs

1) Four-Port Converter:

By combining the two BDCs with a port shared, the derived FB-BDC-MPC topologies have four ports totally, and a family of four-port converters can be harvested, as shown in Fig. 7. In each of the resulted topologies, all the three sources, *U*1, *U*2, and *U*3, can supply power to the load, *Uo*, and the power can also be exchanged simultaneously between *U*1 and *U*2/*U*3 because the two BDCs on the primary side of the converter build a bidirectional three port converter. Single-stage conversion between *U*1 and *U*2 and *U*1 and *U*3 can be achieved with the bidirectional three-port converter on the primary side. However, the conversion between *U*2 and *U*3 is a two-stage one.

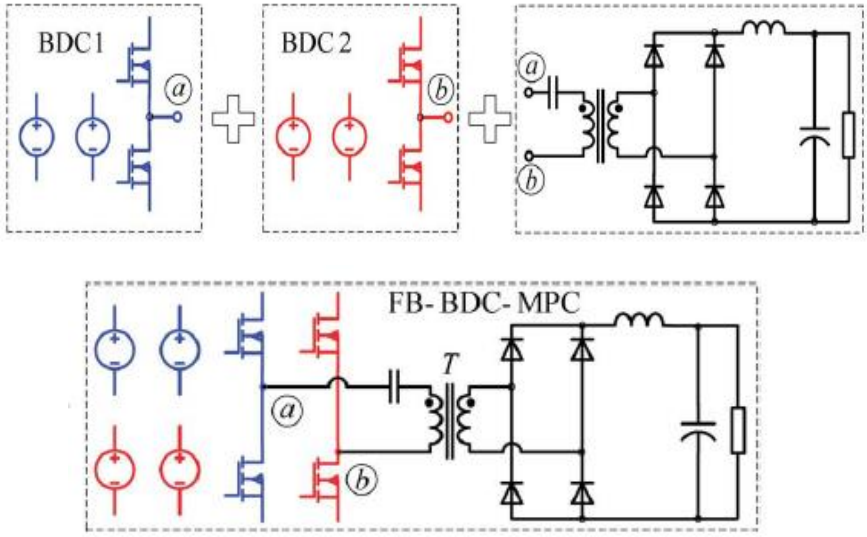

Fig.5. Generation of the FB-BDC-MPC

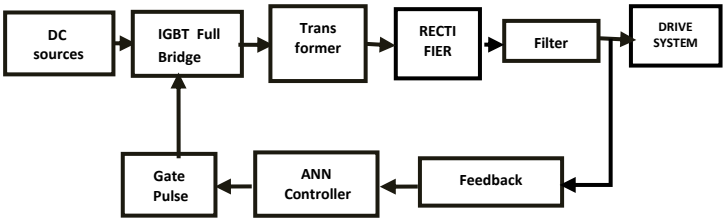

Fig.6. Block diagram of the proposed converter

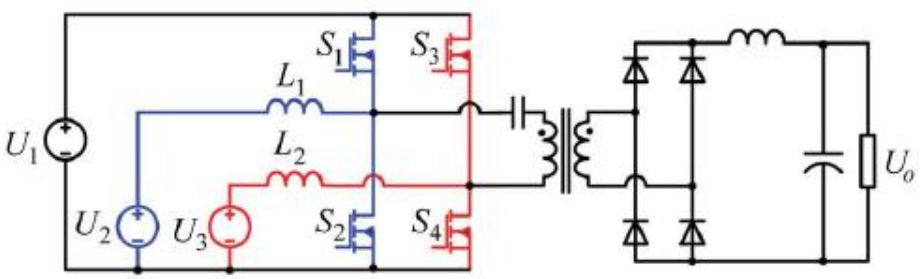

Fig.7 Four port converter derived from Buck/ Boost BDC

III. ANALYSIS ON THE FPC

The BB-FPC shown in Fig. 7 is taken as an example to verify the validity of the proposed topologies. This converter is applied to a PV and WT-sourced system with a battery backup for servo application, as shown in Fig. 8. As illustrated in Fig.8, L_k is the leakage inductance of the transformer. The switches S_1 and S_2 and the inductor L_1 form a boost converter to interface the PV panel PV_1 with the battery. The switches *S*3 and *S*4 and the inductor L_2 form another boost converter to interface the PV panel WT or PV2 with the battery. Since the equivalent circuit from PV to the battery is a boost converter, the PV voltage must be lower than the battery voltage. In addition, the switches $S_1 - S_4$, the transformer *T*, the output diodes *Do*1 − *Do*4, the output filter inductor *Lo*, and the output capacitor *Co* compose a PS-FBC, which can supply power to the isolated load *uo*

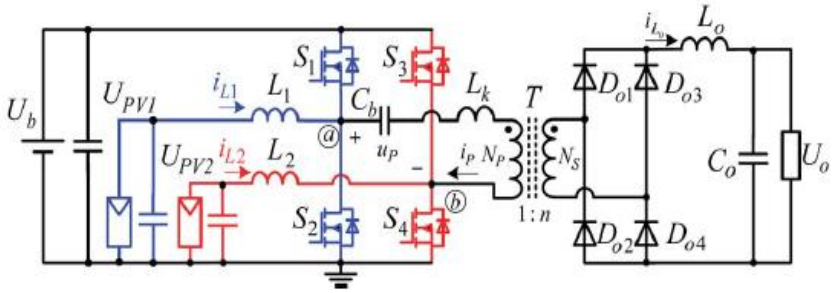

Fig.8. Four Port Converter

A. Switching State

The key waveforms of the proposed BB-FPC have been shown in Fig. 10, where the two switches of each leg are operated in complementary to generate a rectangular voltage from the midpoint of the leg. Duty cycles of *S*2(*S*1) and *S*4(*S*3) are adopted as two control variables to control the power exchanging between the PV1 and the battery and the WTor PV_2 and the battery, respectively. Furthermore, the two rectangular-wave voltages, *ua* and *ub*, the outputs from the midpoints of the two legs, are in phase shift with an angle ϕ to control and regulate the output voltage *Uo*.

Define the turns ratio of the transformer as *NP* : *NS* = 1 : *n* and the voltage on the block capacitor *Cb* as *U*Cb. There are six switching states in one switching cycle. The equivalent circuit in each switching state is shown in Fig. 9.

State I [*t*0 − *t*1] [refer to Fig. 9(a)]: At *t*0, *S*1 is turned off, *S*2 is turned on, and *S*3 remains on. *L*1 begins to be charged, and *L*2 is still discharged linearly. The filter inductor current, *i*Lo, freewheels through the rectifier diodes,*Do*1 − *Do*4, and the secondary windings of the transformer is shorted by the rectifier diodes

$$\frac{di_P}{dt} = -\frac{U_b + U_{\mathrm{Cb}}}{L_k}. \qquad (1)$$

State II [*t*1 − *t*2] [refer to Fig. 9(b)]: At *t*2, *ip* = −*ni*Lo, and *Do*1 and *Do*4 bear reverse bias. The primary sources supply power to the load through the transformer. The important equations of this state are as follows:

$$\begin{cases} \frac{di_{L1}}{dt} = \frac{U_{\mathrm{PV1}}}{L_1} \\ \frac{di_{L2}}{dt} = \frac{U_{\mathrm{PV2}} - U_b}{L_2} \\ \frac{di_{\mathrm{Lo}}}{dt} = \frac{n[U_b + U_{\mathrm{Cb}}] - U_o}{L_o}. \end{cases} \qquad (2)$$

The drain-to-source currents through *S*2 and *S*3 are

$$\begin{cases} i_{S2}(t) = i_{L1}(t) + ni_{\mathrm{Lo}}(t) \\ i_{S3}(t) = -i_{L2}(t) + ni_{\mathrm{Lo}}(t). \end{cases} \qquad (3)$$

State III [*t*2 − *t*3] [refer to Fig. 9(c)]: At *t*2, *S*3 is turned off, *S*4 is turned on, and *S*2 remains on. *iL*2 starts to increase, and the voltage of the block capacitor *Cb*, *U*Cb, applies on the transformer primary windings

$$\begin{cases} \frac{di_{L1}}{dt} = \frac{U_{\mathrm{PV1}}}{L_1} \\ \frac{di_{L2}}{dt} = \frac{U_{\mathrm{PV2}}}{L_2} \\ \frac{di_{\mathrm{Lo}}}{dt} = \frac{nU_{\mathrm{Cb}} - U_o}{L_o}. \end{cases} \qquad (4)$$

The drain-to-source current through *S*4 is

$$i_{S4}(t) = i_{L2}(t) - ni_{\mathrm{Lo}}(t). \tag{5}$$

State IV [*t*3 − *t*4] [refer to Fig. 9(d)]: At *t*3, *S*2 is turned off, *S*1 is turned on, and *S*4 remains on. *L*1 begins to be discharged, and *L*2 is still charged linearly. *i*Lo begins to freewheel through the rectifier diodes, *Do*1 − *Do*4, and the voltage applied on the leakage inductance *Lk* is (*Ub* − *U*Cb)

$$\frac{di_P}{dt} = \frac{U_b - U_{\mathrm{Cb}}}{L_k}. \tag{6}$$

State V [*t*4 − *t*5] [refer to Fig. 9(e)]: In this state, *Do*2 and *Do*3 bear reverse bias. The filter inductor current *i*Lo fully flows through *Do*1 and *Do*4

$$\begin{cases} \frac{di_{L1}}{dt} = \frac{U_{\mathrm{PV1}} - U_b}{L_1} \\ \frac{di_{L2}}{dt} = \frac{U_{\mathrm{PV2}}}{L_2} \\ \frac{di_{\mathrm{Lo}}}{dt} = \frac{n[U_b - U_{\mathrm{Cb}}] - U_o}{L_o}. \end{cases} \tag{7}$$

The drain-to-source currents through *S*1 and *S*4 are

$$\begin{cases} i_{S2}(t) = -i_{L1}(t) + ni_{\mathrm{Lo}}(t) \\ i_{S4}(t) = i_{L2}(t) + ni_{\mathrm{Lo}}(t). \end{cases} \tag{8}$$

State VI [*t*5 − *t*6] [refer to Fig. 9(f)]: At *t*5, *S*4 is turned off, *S*3 is turned on, and *S*1 remains on. *U*Cb applies on the transformer primary windings, *iL*2 begins to decrease, and *i*Lo flows through *Do*1 and *Do*4

$$\begin{cases} \frac{di_P}{dt} = -\frac{U_{\mathrm{Cb}}}{L_k} \\ \frac{di_{L1}}{dt} = \frac{U_{\mathrm{PV1}} - U_b}{L_1} \\ \frac{di_{L2}}{dt} = \frac{U_{\mathrm{PV2}} - U_b}{L_2} \\ \frac{di_{\mathrm{Lo}}}{dt} = -\frac{U_o}{L_o}. \end{cases} \tag{9}$$

The drain-to-source current through *S*3 is

$$i_{S4}(t) = -i_{L2}(t) - ni_{\mathrm{Lo}}(t). \tag{10}$$

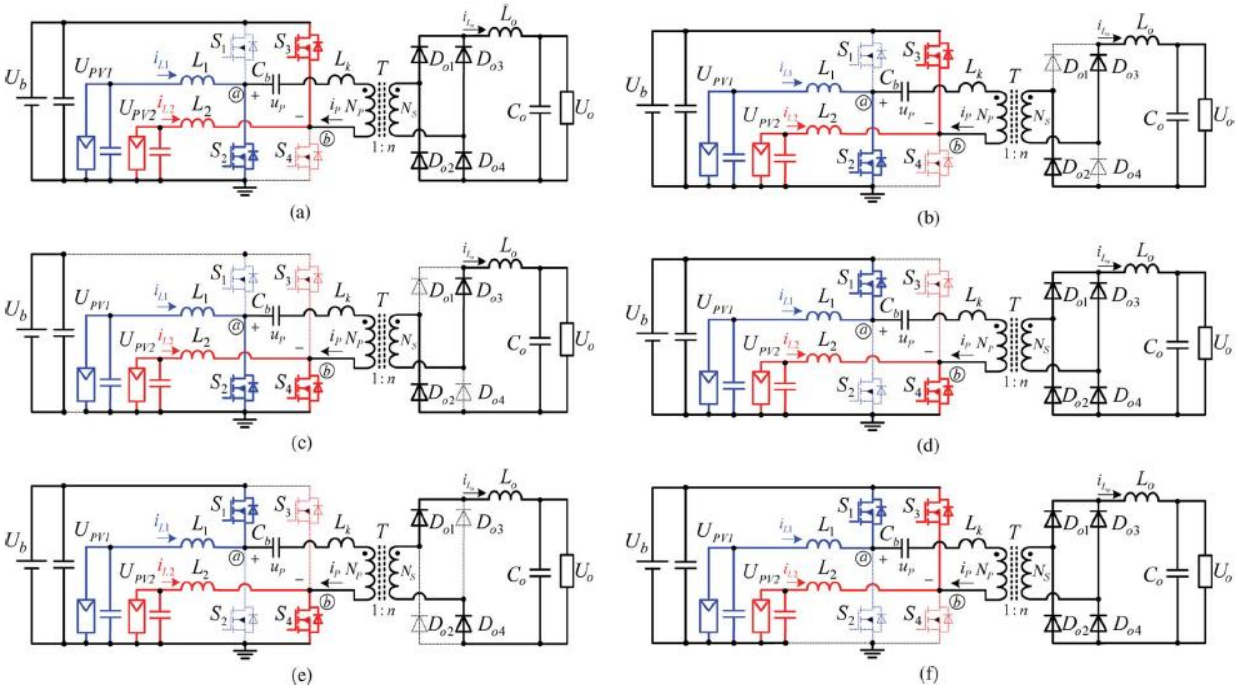

Fig.9. Equivalent circuits in different switching state

$$U_{\mathrm{Cb}} = \int_0^{T_S} u_p dt = U_b \left[\left(D_{\mathrm{PV2}} + \frac{\varphi}{2\pi} - D_{\mathrm{PV1}} \right) - \frac{\varphi}{2\pi} \right]$$
$$= U_b (D_{\mathrm{PV2}} - D_{\mathrm{PV1}})$$
$$= U_b \Delta D_{\mathrm{PV21}} \qquad (11)$$

Where $\Delta D\mathrm{PV21} = D\mathrm{PV2} - D\mathrm{PV1}$. By ignoring the current ripple on the output filter inductor *Lo* and applying the charge balance principle on the block capacitor, the dc bias current *I*bias flowing through the transformer can be derived by

$$(nI_o - I_{\mathrm{bias}}) D_{\mathrm{PV1}} = (1 - D_{\mathrm{PV1}})(nI_o + I_{\mathrm{bias}}). \qquad (12)$$

It can be rewritten as

$$I_{\mathrm{bias}} = (2D_{\mathrm{PV1}} - 1) nI_o = (2D_{\mathrm{PV1}} - 1) n \frac{P_o}{U_o}. \qquad (13)$$

2) Voltage Conversion Ratio: Define the phase angle shift between the turn-on time of *S*2 and *S*4 as ϕ, as shown in Fig. 10. Because the equivalent circuit between the PV and the battery is a boost converter, we have

$$U_b = \frac{U_{\mathrm{PV1}}}{1 - D_{\mathrm{PV1}}} = \frac{U_{\mathrm{PV2}}}{1 - D_{\mathrm{PV2}}}. \qquad (14)$$

It can be rewritten as

$$\begin{cases} U_{\mathrm{PV1}} = (1 - D_{\mathrm{PV1}}) U_b \\ U_{\mathrm{PV2}} = (1 - D_{\mathrm{PV2}}) U_b. \end{cases} \qquad (15)$$

According to the switching states of the converter, as illustrated in Fig. 10, and by applying the volt–second balance principle on the filter inductor *Lo*, we have

(a) [*t*0 − *t*1], (b) [*t*1 − *t*2], (c) [*t*2 − *t*3], (d) [*t*3 − *t*4], (e) [*t*4 − *t*5], and (f) [*t*5 − *t*6].

$$U_o = n \left\{ \frac{\varphi}{2\pi} (U_b + U_{\mathrm{Cb}}) + \left(D_{\mathrm{PV2}} - D_{\mathrm{PV1}} + \frac{\varphi}{2\pi} \right) (U_b - U_{\mathrm{Cb}}) \right.$$
$$\left. + \left[1 - \left(\frac{\varphi}{2\pi} + D_{\mathrm{PV2}} - D_{\mathrm{PV1}} + \frac{\varphi}{2\pi} \right) \right] |U_{\mathrm{Cb}}| \right\}$$
$$= \begin{cases} nU_b \left[\frac{\varphi}{\pi} (1 - \Delta D_{\mathrm{PV21}}) \right. \\ \qquad \left. + 2\Delta D_{\mathrm{PV21}} - 2\Delta D_{\mathrm{PV21}}^2 \right], & \Delta D_{\mathrm{PV21}} > 0 \\ nU_b \left[\frac{\varphi}{\pi} (1 + \Delta D_{\mathrm{PV21}}) \right], & \Delta D_{\mathrm{PV21}} < 0. \end{cases} \qquad (16)$$

According to (15) and (16), the duty cycles *D*PV and D_{TW} can be employed to balance the PV and the battery powers, and the phase angle ϕ can be adopted to regulate the output voltage on the secondary side. These three control freedoms make the four-variable system fully controllable. In addition, as shown in Fig. 10, to make sure the phase angle ϕ is controllable, there is a constraint

$$\begin{cases} \frac{\varphi}{2\pi} \le D_{\mathrm{PV1}} \\ D_{\mathrm{PV2}} + \frac{\varphi}{2\pi} - D_{\mathrm{PV1}} \le 1 - D_{\mathrm{PV1}}. \end{cases} \qquad (17)$$

It can be rewritten as

$$\frac{\varphi}{2\pi} \le D_{\mathrm{PV1}} \quad \text{and} \quad \frac{\varphi}{2\pi} \le 1 - D_{\mathrm{PV2}}. \qquad (18)$$

It is obvious and can be seen from Fig. 10 that the output voltage *Uo* cannot be regulated by the phase angle ϕ if the constraint condition cannot be satisfied, in which the control variable corresponding to the output voltage is lost.

3) ZVS Analysis: ZVS can be achieved with the help of phase-angle-shift control strategy, which is similar to that of the conventional PS-FBC. If the input power of PV and WT is zero, with the help of *L*1 and *L*2, all the switches can achieve ZVS independent of input voltage and load conditions. However, when the PVs' power is not zero, there will be dc current flowing through *L*1 and *L*2, and this condition will change the ZVS conditions of the low-side switches, *S*2 and

*S*4. It means that only the high-side switches, *S*1 and *S*3, can always achieve ZVS, and *S*2 and *S*4 can achieve ZVS under certain conditions.

For simplicity, ignore the current ripple of filter inductor *Lo*, and assume that all the switches' output capacitance is *C*oss.

According to the switching state III, when *S*3 is turned off at *t*2, the current flowing through *S*4 is determined by (5). Thus, the ZVS of *S*4 can be obtained if this current is negative

$$I_{L2} - nI_o < 0 \qquad (19)$$

where *Io* is the load current and *IL*2 is the average current of *L*2. As a result, the detailed ZVS condition of switch *S*4 can be derived as

$$P_{TW} < \frac{U_{TW}\ nP_o}{U_o}. \qquad (20)$$

From (20), it can be seen that the larger *Po* and the smaller P_{TW}, the easier *S*4 can achieve ZVS.

Switch *S*2 cannot achieve ZVS easily because, when *S*1 is turned off, the output filter inductor on the secondary side is in the freewheeling state, as depicted in Fig. 12(a), and no current is reflected to the primary side. As a result, when *S*1 is turned off at *t*0, only the energy stored in the leakage inductance can be utilized to achieve the ZVS of *S*2. Thus, the prerequisite for *S*2 ZVS is *iL*1(*t*0) > 0. Another condition is that the energy stored in the leakage inductance can discharge the drain-to source voltage of *S*2 to zero. Therefore, the ZVS condition of *S*2 can be derived as

$$\left(n\frac{P_o}{U_o}\right)^2 > \frac{2U_b C_{oss}^2}{L_k} + \left(\frac{P_{PV1}}{U_{PV1}}\right)^2 \quad \text{and} \quad n\frac{P_o}{U_o} > \frac{P_{PV1}}{U_{PV1}}. \qquad (21)$$

From (21), it can be seen that the larger *Po* and *Lk* and the smaller *P*PV1, the easier *S*2 can achieve ZVS. On the other hand, if *iL*1(*t*0) < 0, *S*2 can also be turned on with ZVS with the help of the energy stored in *L*1.

IV. MODULATION AND CONTROL

A. Modulation Scheme and Analysis:

A PWM and PSM scheme is applied to the BB-FPC. As shown in Fig. 11, *D*PV1 is the duty cycle of switch *S*2 and regulated by control voltage *u*DPV1, *D*PV2 is the duty cycle of switch *S*4 and regulated by control voltage *u*DPV2, *u*tri1 and *u*tri2 are the two carrier voltages,

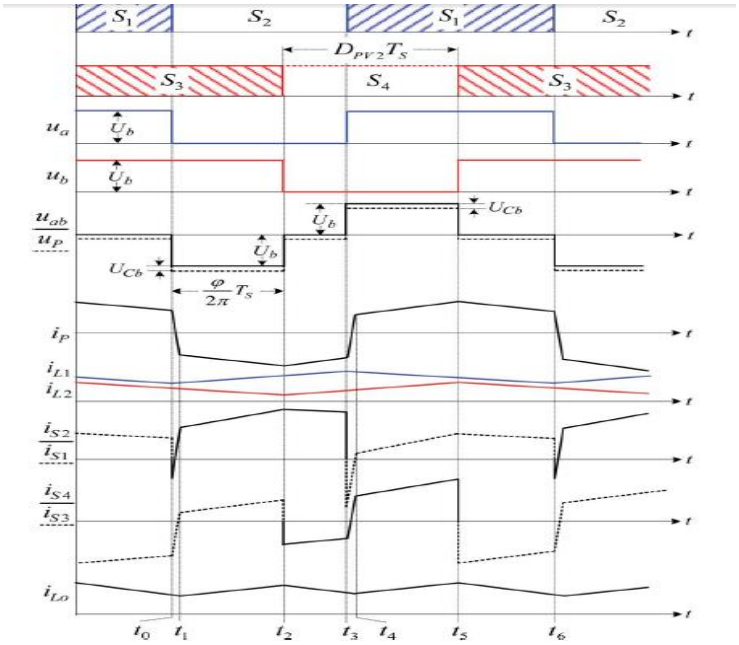

Fig.10. Wave form of the BB- FPC

ϕ is the phase angle between *u*tri1 and *u*tri2 and regulated by control voltage *ur*ϕ, and *TS* is the switching period. As shown in Fig. 13, *D*PV1 is employed as one of the control freedoms to accurately balance the power and voltage between PV1 and the battery, *D*PV2 is employed as another control freedom to balance the power and voltage between PV2 and the battery, and the phase angle ϕ is adopted as the third control freedom to balance the voltage between the battery and load.

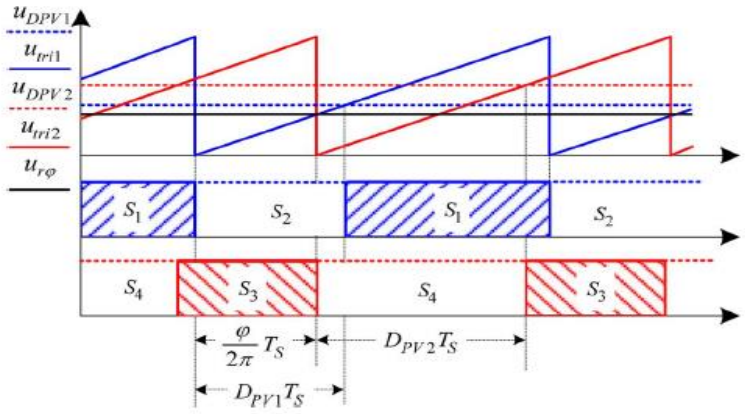

Fig.11. Modulation scheme

According to the derivation process and operation principles of the BB-FPC, the equivalent circuit between the PV and the battery is a conventional boost converter, and the equivalent circuit between the battery and the load is a PS-FBC. With the modulation scheme shown in Fig. 11, the control of the boost converter and that of the PS-FBC are independent of each other. The battery acts as the output of the boost converter and input of the PS-FBC, which means that the PV and load is decoupled by the battery. As a result, the BB-FPC is equivalent to a conventional cascade solution shown in Fig. 12.

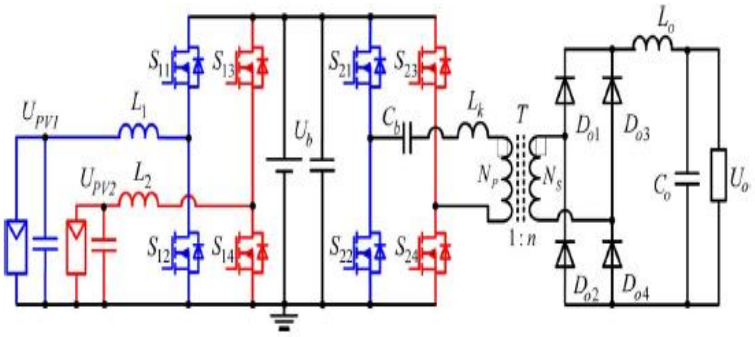

Fig.12. Equivalent circuit of the proposed BB-FPC

where two boost converters and one PS-FBC are employed. However, the power from the PV to the load has to be converted two times with the conventional solution shown in Fig. 12, which leads to higher power losses than the integrated solution with BB-FPC.

Dynamic modeling can be carried out using conventional averaging techniques. Considering that, the BB-FPC can be decoupled to two boost converters and a PS-FBC, and the modeling processes of these two types converters have been carried out in many literatures. Thus, the detailed dynamic modeling process of the BB-FPC, which is not the main focus of this paper, will not be presented. The control-to-input-voltage transfer function for the equivalent boost converter in the BB-FPC can be given by

$$G_{\text{ci-dc}} = -\frac{U_b}{L_x C_{\text{PVx}}} \frac{1}{s^2 + \frac{1}{r_{\text{PVx}} C_{\text{PVx}}} s + \frac{1}{L_x C_{\text{PVx}}}} \qquad (22)$$

Where *Lx* and *C*PVx are the filter inductor and input capacitor of the related boost converter and *r*PVx is the dynamic resistance of the PV. The negative gain in implies that the stable PV control requires a positive feedback of the input voltage.

B. Operation Modes and Analysis:

The operation of the PV–battery power system is categorized into five modes.

Mode I: The PV power is zero, and the battery discharges to supply power to the load alone. This mode is also named single-input single-output mode.

Mode II: In this mode, the generated PV power is less than the load demands. Both PV and battery supply power to the load. The two PVs both operate in MPPT state. This mode is also named dual-input mode.

Mode III: In this mode, the generated PV power is greater than the load demands. The PVs operate in MPPT state, and the battery absorbs all the surplus PV power.

Mode IV: In this mode, the maximum generated PV power is greater than the total of the load and battery charging demands. The battery may operate in CC or CV charging state. Only one PV module operates in MPPT state, and the other one does not operate in the MPPT state.

Mode V: In this mode, the maximum generated PV power is greater than the total of the load and battery charging demands. The battery may operate in CC or CV charging state. Both the two PV modules do not operate in MPPT state. Modes III, IV, and V are also named dual-output mode.

The operation states of the PVs and battery in different modes have been listed in Table I.

TABLE I
OPERATION STATES OF PVS AND BATTERY IN DIFFERENT MODES

Mode	PV1	PV2	Battery
I	N/A	N/A	Discharging
II	MPPT	MPPT	Discharging
III	MPPT	MPPT	Charging
IV	MPPT	Not MPPT	CC/CV Charging
V	Not MPPT	Not MPPT	CC/CV Charging

C. Power Management and Feedback Control:

The key of the power management of the PV–battery power system is to balance the power between PV and the battery while maximizing the utilization of PV power. To balance the power among the two PVs, the battery, and the load, the designed power management and feedback controller is shown in Fig. 13. The PV MPPT control, battery charging control, battery discharging control, and load voltage control have been taken into account in the power management.

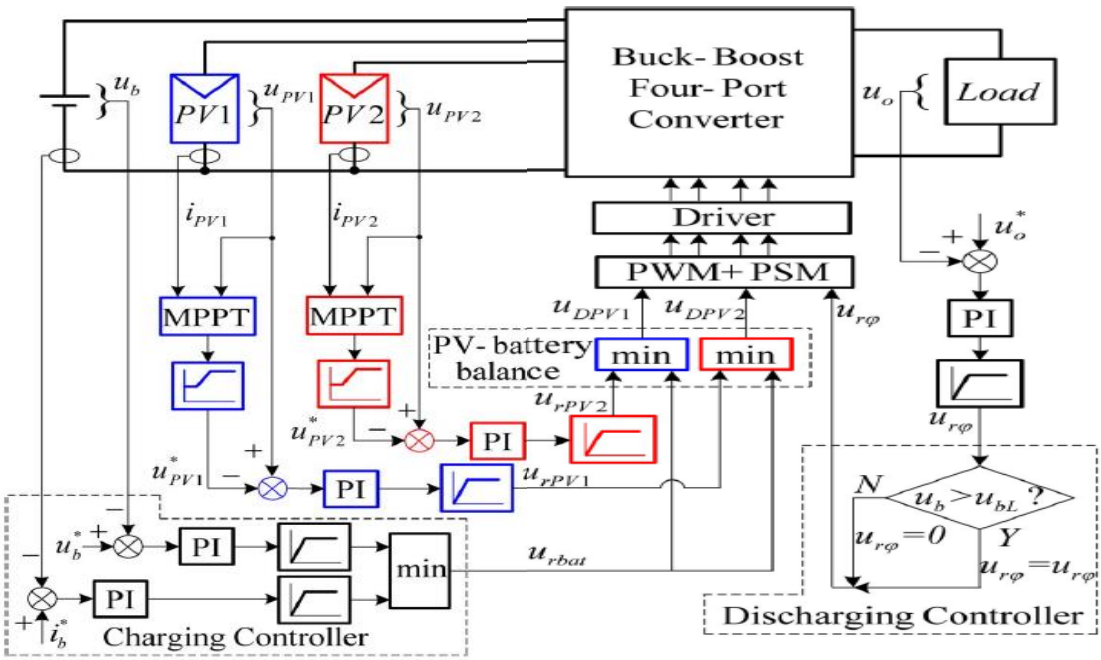

Fig.13. Control block diagram of the FPC

The load voltage loop is simply a voltage-mode control loop. According to the dc circuit equation shown in (16), the output voltage *Uo* can be controlled by the phase shift angle ϕ since battery voltage is almost constant. On the other hand, according to the dc circuit equation shown in (15), duty cycles *D*PV1 and *D*PV2 are assigned to balance the power among the two PVs and the battery.

The CC and the CV charging are taken into consideration in the battery charging control. A discharging controller is employed to shut down the load power by setting the phase shift angle to be zero once the battery voltage is lower than a low state of charge level. The MPPT controller is used to regulate the PV voltages to their reference value since battery voltage *Ub* is almost constant.

The PV voltage references are provided by the MPPT controller using the perturb-and-observe algorithm.

In order to utilize the PV power sufficiently and balance the power among the PVs and the battery, an autonomous mode transition is employed with a competitive manor. As shown in Fig. 13, the battery charging control voltage, *u*rbat, and PV MPPT control voltages, *u*rPV1 and *u*rPV2, run in parallel to compete for the minimum value in order to win control over *D*PV1 and *D*PV2. To clearly describe the implementation of power balance between PVs and the battery when the converter operates in Modes II to V, the relations among the three control voltages in different operation modes are shown in Fig. 14.

Fig. 14(a) shows Mode II, where the available total maximum PV power is less than the load power and the insufficient power will be automatically supplied by the discharge of the battery. Fig. 14(b) shows Mode III, where the available total maximum PV power is greater than the load power and the surplus PV power is charged to the battery, but the charging current and voltage are less than the preset commands ($i * b$ and $u * b$). Therefore, in Modes I and II, the control voltage generated by the battery charging controller, *u*rbat, which is a proportional and integral controller, will go positive and be limited at the maximum value. It results that the voltage commands *u*DPV1 and *u*DPV2 are determined by the two MPPT controller, and thus, both the two PV modules are operated in the MPPT state. Once the available maximum PV power is greater than the battery charging and load requirement, *u*rbat will go negative until the power balance among the two PVs and the battery is achieved. Fig. 14 shows Mode III, where the maximum power point voltage of PV2 is smaller than that of PV1, and when *u*rbat goes negative, it will become smaller than *u*rPV2 first and replace *u*rPV2 to be the control input of *D*PV2. As a result, PV2 will disable the MPPT, and *u*rPV2 goes positive and then will be limited at the maximum value because the voltage of PV2 is shifted to a higher level by *u*rbat. If the power balance is achieved, *u*rbat will stop going negative. Thus, only the PV with a higher maximum power point voltage will operate at the MPPT state, and the other PV will not operate at the MPPT state. Once the PV power increases continuously or the load power decreases, the desired PV power will also decrease. This will lead to *u*rbat going negative gain until *u*rbat is smaller than *u*rPV1 and replace *u*rPV1 to be the control input of *D*PV1. As a result, PV1 will also disable the MPPT, and *u*rPV1 will go positive and then be limited at the maximum value. This is the operation of Mode IV, as shown in Fig. 14. In this mode, the voltages of the two PV modules are the same because both *D*PV1 and *D*PV2 are regulated by *u*rbat.

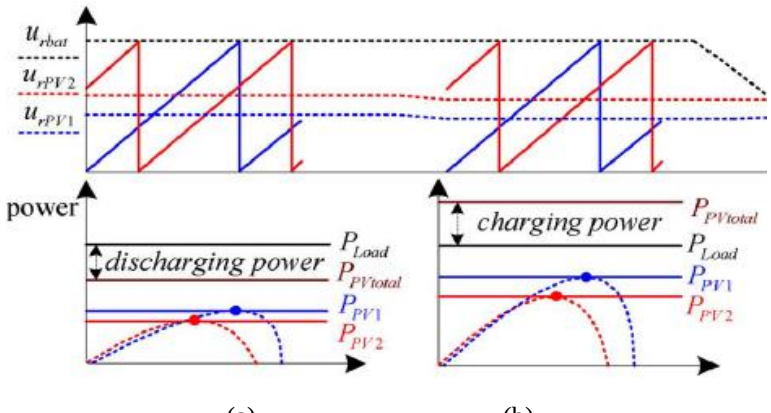

(a) (b)

Fig.14 Power balance among the PV and Battery

With the control schemes shown in Fig. 13, the MPPT control of the PV modules is disabled only when the available PV power is greater than the total power for battery charging and load requirement. This scheme can guarantee the most sufficient utilization of PV power. What is more, the battery will not be overcharged or over discharge.

V. EXPERIMENTAL VERIFICATIONS

A. Experimental Results and Analysis:

The steady-state waveforms of the BB-FPC operating in Mode III are shown in Fig. 18. The testing conditions are as follows: battery voltage *Ub* = 72 V, PV voltages *U*PV = 12 V and *U*w = 12 V, PV powers *P*PV = 100 W and wind = 50 W, and output load power *Po* = 110 W. In this case, both the load and battery take power from the two PV sources. The total input power is about 150 W, and the surplus power is charged to the battery.

The ZVS turn-on waveforms of the switches *S*2 and *S*4 are shown in Fig. 16, where the ZVS turn-on of *S*2 and *S*4 has been achieved. As analyzed earlier, the two high-side switches, *S*1 and *S*3, have similar soft-switching performance and can always achieve ZVS turn-on. Therefore, all the primary switches can operate under soft-switching conditions to reduce the switching losses.

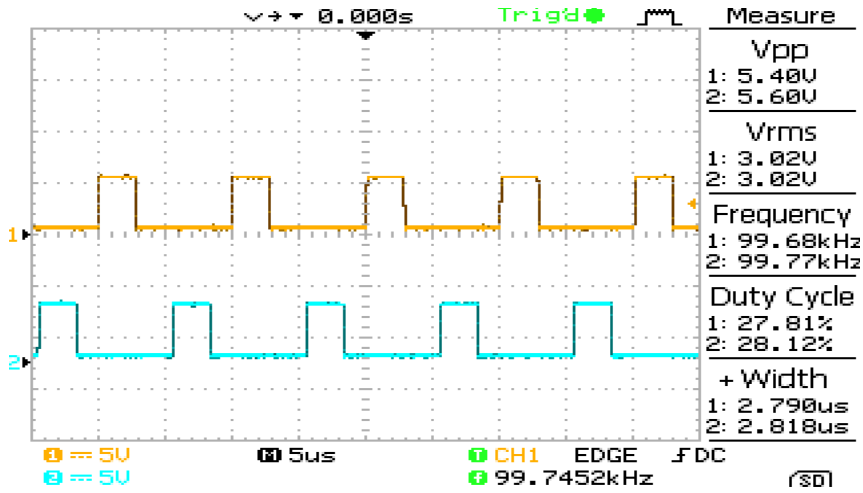

(a)

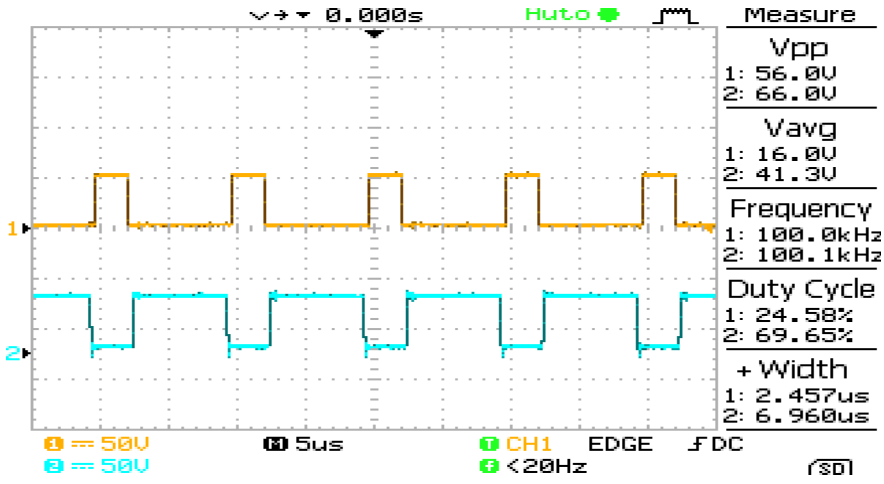

(b)

Fig.15. Steady state waveforms

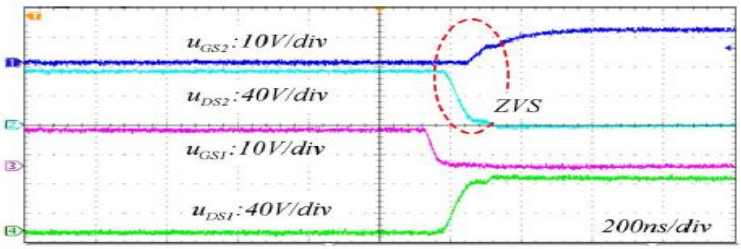

Fig.16. ZVS waveforms of S_2 and S3

When the power is transferred from the PV to the load, the efficiency comparison between the BB-FPC, which is shown in Fig. 14, and the conventional boost cascade FBC solution is shown in Fig. 17. It is obvious that, under the same testing conditions, a higher efficiency can be achieved with the integrated BB-FBC since single-stage conversion can be achieved.

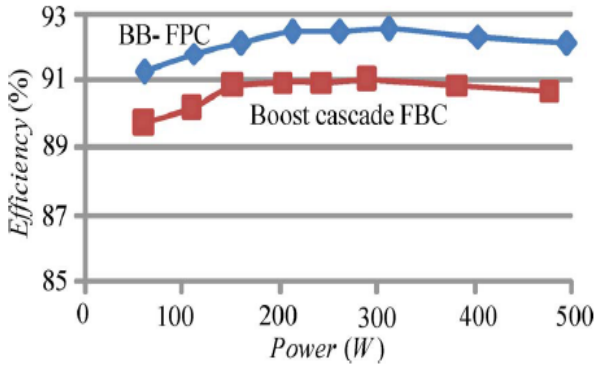

Fig.17. Efficiency Comparison between the BB-FPC and the Conventional solution when power is transferred from PV to the load.

VI. CONCLUSION

In this paper, a systematic method for synthesizing MPCs from FBC and BDCs has been proposed. The switching legs parasitized in the BDCs have been found and shared with the FBC to derive families of FB-BDC-MPCs. The proposed FB-BDC-MPCs are capable of interfacing multiple bidirectional sources and isolated output load simultaneously.

Single-stage power conversion between any two ports and ZVS of all the active switches have been achieved in the proposed MPCs. These result in high conversion efficiency.

All the port voltages are controlled simultaneously by employing PWM and phase angle- shift control scheme. These topologies are good candidates for renewable power systems as interface converters due to their advantages of simple configuration, reduced devices, and easy control. A typical four-port converter developed by the proposed method, named as BB-FPC, is analyzed and implemented as an example, with detailed operation principles, design considerations, modulation, and power management strategies presented. Experimental results on a 500-W prototype of BB-FPC with good steady-state and dynamic performances demonstrate the feasibility and effectiveness of the proposed method.

The proposed FB-BDC-MPCs offer alternate solutions for renewable power systems with multi-input renewable sources, with storage backups, or with hybrid storage units. These renewable power systems can be applied in electric Drives or stand-alone micro grid.

REFERENCES

[1] H. Fakham, D. Lu, and B. Francois, "Power control design of a battery charger in a hybrid active PV generator for load-following applications," *IEEE Trans. Ind. Electron.*, vol. 58, no. 1, pp. 85–94, Jan. 2011.

[2] T. Hirose and H. Matsuo, "Standalone hybrid wind-solar power generation system applying dump power control without dump load," *IEEE Trans.Ind. Electron.*, vol. 59, no. 2, pp. 988–997, Feb. 2012.

[3] W. Jiang and B. Fahimi, "Multiport power electronic interface—Concept,modeling and design," *IEEE Trans. Power Electron.*, vol. 26, no. 7, pp. 1890–1900, Jul. 2011.

[4] H. Tao, J. L. Duarte, and M. A. M. Hendrix, "Multiport converters for hybrid power sources," in *Proc. IEEE PESC*, 2008, pp. 3412–3418.

[5] H. Tao, J. L. Duarte, andM. A.M. Hendrix, "Three-port triple-half-bridge bidirectional converter with zero-voltage switching," *IEEE Trans. Power Electron.*, vol. 23, no. 2, pp. 782–792, Mar. 2008.

[6] H. Tao, A. Kotsopoulos, J. Duarte, andM. Hendrix, "Transformer coupled multiport ZVS bidirectional dc-dc converter with wide inputrange," *IEEE Trans. Power Electron.*, vol. 23, no. 2, pp. 771–781, Mar. 2008.

[7] K. Haribaran and N. Mohan, "Three-port series- resonant dc-dc converter to interface enewable energy sources with bidirectional load and energy storage ports," *IEEE Trans. Power Electron.*, vol. 24, no. 10, pp. 2289–2297, Oct. 2009.

[8] T. Zhou and B. Francois, "Energy management and power control of a hybrid active wind generator for distributed power generation and grid integration," *IEEE Trans. Ind. Electron.*, vol. 58, no. 1, pp. 95–104, Jan. 2011.

[9] T. Bhattacharya, V. S. Giri, K. Mathew, and L. Umanand, "Multiphase bidirectional flyback converter topology for hybrid electric vehicles," *IEEE Trans. Ind. Electron.*, vol. 56, no. 1, pp. 78–84, Jan. 2009.

[10] X. Liu, P. Wang, P. C. Loh, and F. Blaabjerg, "A compact three-phase single-input/dual-output matrix converter," *IEEE Trans. Ind. Electron.*, vol. 59, no. 1, pp. 6–16, Jan. 2012.

[11] Xu, C. Zhao, and H. Fan, "A PWM plus phase-shift control bidirectional dc-dc converter," *IEEE Trans. Power Electron.*, vol. 19, no. 3, pp. 666–675, May 2004.

[12] P. K. Jain, W. Kang, H. Soin, and Y. Xi, "Analysis and design considerations of a load and line independent zero voltage switching full bridge dc/dc converter topology," *IEEE Trans. Power Electron.*, vol. 17, no. 5, pp. 649–657, Sep. 2002.

NOMENCLATURE

BB-FPC	Buck/boost four-port converter	MPPT	Maximum power point tracking
BDC	Bidirectional dc–dc converter	PS-FBC	Phase-shift full-bridge converter
CC	Constant current	PSM	Phase shift modulation
CV	Constant voltage	PV	Photovoltaic
FBC	Full-bridge converter	PV, WT	Inputs
FB-BDC-MPC	Full-bridge and bidirectional dc-dc converter-based multiport converter	PWM	Pulse width modulation
		ZVS	Zero-voltage switching.
MPC	Multiport converter		